Petroleum Science (2021) 18:852–869
https://doi.org/10.1007/s12182-020-00538-7

ORIGINAL PAPER

Experimental study of enhanced oil recovery by CO_2 huff-n-puff in shales and tight sandstones with fractures

Chao-Fan Zhu[1,2] · Wei Guo[1] · You-Ping Wang[3] · Ya-Jun Li[2] · Hou-Jian Gong[2] · Long Xu[2] · Ming-Zhe Dong[2,4]

Received: 11 August 2020 / Accepted: 12 November 2020 / Published online: 5 December 2020

Abstract

The fractures and kerogen, which generally exist in the shale, are significant to the CO_2 huff-n-puff in the shale reservoir. It is important to study the effects of fractures and kerogen on oil recovery during CO_2 huff-n-puff operations in the fracture–matrix system. In this study, a modified CO_2 huff-n-puff experiment method is developed to estimate the recovery factors and the CO_2 injectivity in the fractured organic-rich shales and tight sandstones. The effects of rock properties, injection pressure, and injection time on the recovery factors and CO_2 usage efficiency in shales and sandstones are discussed, respectively. The results show that although the CO_2 injectivity in the shale is higher than that in the sandstone with the same porosity; besides, the recovery factors of two shale samples are much lower than that of two sandstone samples. This demonstrates that compared with the tight sandstone, more cycles are needed for the shale to reach a higher recovery factor. Furthermore, there are optimal injection pressures (close to the minimum miscible pressure) and CO_2 injection volumes for CO_2 huff-n-puff in the shale. Since the optimal CO_2 injection volume in the shale is higher than that in the sandstone, more injection time is needed to enhance the oil recovery in the shale. There is a reference sense for CO_2 huff-n-puff in the fractured shale oil reservoir for enhanced oil recovery (EOR) purposes.

Keywords Shale · Tight sandstone · CO_2 huff-n-puff · Fracture · Injectivity of CO_2

1 Introduction

In recent years, the majority of newly discovered oil reservoirs are unconventional reservoirs. Shale oil reservoirs have been discovered in the Bakken Formation (3.65 billion barrels), Three Forks (3.73 billion barrels), Appalachian, Gulf of Mexico, west Siberian, Songliao, and Ordos basins around the world (Gaswirth and Marra 2015). There is a strong consensus that oil can be produced from certain fractured shale oil reservoirs (Zou and Yang 2013). Similar to the tight sandstone, the shale has very pore storage and permeable property, which is adverse to the production (Bustin and Bustin 2012; McGlade et al. 2013). Besides, because shales are rich in kerogen (Wang et al. 2019), the oil in shale consists of free, adsorbed, and dissolved oil (Yang et al. 2016; Zhu et al. 2018b). Molecular simulation results show that the affinity of oil and kerogen is larger than gas, oil cannot be desorbed even at atmospheric pressure (Falk et al. 2015; Zhu et al. 2018a). Since the mobility of shale oil is very low, the primary oil recovery factor of the shale oil reservoir is less than 15% (Cherian et al. 2012; Hoffman 2012; Iwere et al. 2012; Yu et al. 2014). Therefore, EOR is necessary to achieve maximum economic efficiency in shale oil reservoirs. However, water flooding cannot be used in shale oil reservoirs because of the clay swelling problems, poor sweep efficiency, and low injectivity (Yu et al. 2015; Ahmad et al. 2019).

The gas injection is an important method in the EOR of the shale reservoir (Li et al. 2018; Jia et al. 2019). Yu and Sheng (2016) investigated that cyclic gas injection provided a steadier and continuous recovery performance

Edited by Yan-Hua Sun

✉ Ming-Zhe Dong
Mingzhe.dong@ucalgary.ca

[1] College of Construction Engineering, Jilin University, Changchun 130026, Jilin, China

[2] School of Petroleum Engineering, China University of Petroleum (East China), Qingdao 266580, China

[3] Petroleum Exploration and Production Research Institute, Sinopec, Beijing 100083, China

[4] Department of Chemical and Petroleum Engineering, University of Calgary, Calgary, AB T2N 1N4, Canada

than cyclic water injection. Sharma and Sheng (2017) compared the recovery factor of methane and ethane huff-n-puff with methyl alcohol and isopropanol huff-n-puff, the result showed that the production rate and ultimate recovery factor of gas huff-n-puff are both best. A series of experiments and simulations have been conducted on the Wolfcamp shale to study the effect of different gases on the gas huff-n-puff in the shale, and the results show that the recovery factor of CO_2 huff-n-puff is better than CH_4 and nitrogen huff-n-puff (Li et al. 2017a). Field tests show that the CO_2 injection causes significant reductions in the interfacial tension and oil viscosity (Gondiken 1987). A greater permeability caused by carbonic acid dissolution of calcium carbonate has been well documented (Torabi and Asghari 2010). Schenewerk et al. (1992) performed a study in South Louisiana and showed that CO_2 huff-n-puff can significantly reduce the water cut in wells and alter the saturation distribution. Besides, the diffusion coefficient of CO_2 in oil is higher than nitrogen and water (Zheng and Yang 2017; Zhu et al. 2018c), and the adsorptive properties of CO_2 in kerogen are greater than those of other gases (Mitchell et al. 2004; Kurniawan et al. 2006; Ottiger et al. 2008; Pollastro et al. 2008). The higher diffusion coefficient and excellent adsorptive properties of CO_2 are beneficial to replacing the adsorption-dissolution oil in the kerogen. The combined effects of fracture impaction, diffusion, and nanopore result in an additional 3.8% of oil production during CO_2 huff-n-puff (Zhang et al. 2018). In conclusion, CO_2 injection is a good EOR method for shale oil production.

The modes of CO_2 injection in EOR can be categorized into three types: huff-n-puff, multiple-well cyclic injection, and continuous injection (Burrows et al. 2020; Iddphonce et al. 2020; Singh 2018). The difference of multiple-well circulation from huff-n-puff is that the injection well and production well of CO_2 injection are separated. Since it can provide beneficial interwell interference, multiple-well circulation may be more effective than huff-n-puff (Kong et al. 2016). The experiment and simulation results showed that the recovery factor of continuous gas injection is larger than huff-n-puff in the homogeneous formation (Wan et al. 2013; Sheng 2015; Yu and Sheng 2015). However, Tovar et al. (2018) demonstrated that the direct gas injection through the shale matrix is not possible in a reasonable time frame. Many technologies, including horizontal wells and multiple hydraulic fracturing, have been used to economically produce shale oil (Daneshy 2009; Gaurav et al. 2012). Although the diffusion coefficient of CO_2 is better than other fluid (Zheng and Yang 2017; Zhu et al. 2018c), the limited influence area of the diffusion mechanism is not enough to compensate for the low velocity caused by the low permeability of the matrix. Therefore, multiple hydraulic fracturing has been used to economically produce shale oil (Daneshy 2009; Gaurav et al. 2012), and huff-n-puff is the best mode of CO_2 injection in the shale reservoir. More CO_2 diffuses into the matrix because of the larger contact area, and CO_2 moves deep because of the higher permeability of fracture.

In recent years, the effects of mechanistic factors (e.g., soaking time, cycle number, pressure) on the CO_2 huff-n-puff in shale cores have been studied by many researchers (Wang et al. 2013; Wan et al. 2013; Li et al. 2017a, b; Sheng 2017; Du et al. 2018). Besides, the effects of heterogeneity (Chen et al. 2014), water saturation (Huang et al. 2020), permeability (Su et al. 2020), pore throat radii and total organic carbon (TOC) content (Hawthorne et al. 2019) on the CO_2 huff-n-puff in the shale were also studied. The recovery factor varies widely (25%–100%), which is caused by different experimental methods and samples. Generally, the recovery factor of shale oil is closely correlated with the injection pressure and contact surface area between CO_2 and rock during CO_2 huff-n-puff in the shale. CO_2 huff-n-puff experiments in the Eagle Ford shale, Marcos shale, and Barnett shale indicated that the oil recovery due to CO_2 injection at pressures at or above the minimum miscibility pressure (MMP) is better than that at pressures below the MMP (Gamadi et al. 2014). The same result was also obtained by Li et al. (2017b) and Hawthorne et al. (2013). Burrows and Haeri (2020) summarized the oil recovery results after 24 h of CO_2 huff-n-puff laboratory testing and the results showed that the recovery factor decreased from 100 to 25% when the core volume/core surface area increased from 0.3 to 10. Therefore, it is important to study the effects of fractures on oil recovery during CO_2 huff-n-puff operations in the fracture–matrix system.

There are three methods to describe the matrix–fracture system in the laboratory. First, a direct visualization experiment with a glass micromodels was used to quantify the recovery rates of oil from fracture networks (Nguyen et al. 2018). Second, a cubic shale sample with an artificial fracture, which is filled with sands and glass beads, was used to model the matrix–fracture system (Tan et al. 2018). Third, a physical model, which is composed of an annular fracture and a cylindrical matrix, was used to study the CO_2 huff-n-puff process in conventional fractured reservoirs (Torabi and Asghari 2010; Sang et al. 2016). In some experiments, the fracture was filled with glass beads to model the fracture with proppant (Tovar et al. 2018). However, these three types of assessment methods have their flaws if employed independently. For the first method, the matrix parts of the glass micromodel are different from the shale matrix; the second model needs a large-scale sample and it is hard to quantitatively describe the fracture; while the fault of the third model is that the fracture is too ideal. Because the samples come from the formation and the size of the core is small, the third model is chosen in this study.

This paper presents an experimental study of the CO_2 huff-n-puff process in shale and sandstone matrix–fracture

systems at high temperatures and pressures. In Sect. 2, a modified experimental method is developed to test the recovery factors of matrix and fracture, respectively, in a special apparatus designed to mimic the CO_2 huff-n-puff process in fractured unconventional formations. Meanwhile, the injectivity of CO_2 in shale and sandstone is calculated accurately by the pressure decline curves. The oil recovery factor of shale with different porosities is compared with sandstone to study the effects of kerogen on CO_2 huff-n-puff. As a result, the effects of injection pressure and injection time on the recovery factors and CO_2 usage efficiency in shale and sandstone are studied.

2 Experimental

2.1 Materials

Four samples were used as the experimental cores, including two shale cores and two sandstone cores. All of the samples were drilled in the Mesozoic Yanchang Formation, Ordos Basin, where a larger number of organic-rich shales were found (Wang 2015). Because the clay content of shale is higher, liquid nitrogen was used as a coolant to cool the shale samples during coring in the laboratory. The hydrocarbon properties of the samples were detected by Rock–Eval pyrolysis (Okiongbo et al. 2005; Tong et al. 2011). The porosities of the samples were tested by the saturation of dodecane (C_{12}), which is the simulated oil in this study. The permeability was tested by the helium (Cui et al. 2009). During the test, the pressures of both ends of the core samples are 16 and 15.5 MPa, respectively. The liquid nitrogen adsorption measurement was used to test the pore volume per mass, specific surface area, and average pore diameter (Sing et al. 1985). According to the BET adsorption theory (Radlinski and Mastalerz 2004), the liquid nitrogen adsorption method was focused on the microporous range (1.7–200 nm). They only indicate the development of the microporous of the samples. Table 1 shows the physical characteristics of the samples and Table 2 shows the physical properties of C_{12} and CO_2. The CO_2–C_{12} phase equilibrium data at 40–70 °C have been studied by Nieuwoudt and Du Rand (2002) and the CO_2–C_{12} system is true first contact miscibility. The MMP in Table 2 is obtained at 60 °C.

Table 2 Physical properties of C_{12} and CO_2 (Lu 1982; Henni et al. 2010; Zhu et al. 2018b, c; Dong et al. 2019)

Fluid	Critical temperature, K	Critical pressure, Pa	Acentric factor	Binary interaction parameter	MMP, MPa
C_{12}	658.2	1.82×10^5	0.673	0.1	13.8
CO_2	304.1	73.7×10^5	0.225		

Figure 1 shows photos of the experimental cores. The cores are approximately 25 mm in diameter and 35–50 mm in length. It should be noted that Sandstone 1 contained many microfractures. As the number of microfractures in oil and gas reservoirs increases, the permeability improves significantly.

In this study, X-ray diffraction analysis (XRD) was used to test the mineral compositions of the samples (Xie et al. 2016). The mineral compositions are listed Table 3. The mineral composition of shale is different from sandstone. The dominant mineral is quartz for sandstones. For shales, the contents of analcite, ankerite, and clay are also higher besides quartz.

2.2 Experimental setup and procedure

An experimental set-up was proposed to test the CO_2 huff-n-puff recovery from oil reservoirs with fractures at high pressures and temperatures. A schematic is shown in Fig. 2, which is comprised of a hydrostatic high-pressure core holder, a confining pressure pump, a CO_2 cylinder, a separator, and a vacuum pump.

The diameter of the core holder was 26.00 mm and the confining pressure pump could provide constant axial pressure on the end face of the core. Therefore, fluid can only flow in a radial direction. The annulus space between the sample and wall of the core holder was used to simulate the fractures. Because the diameter of the core was 25.00 mm, the width of the "fracture" was 0.50 mm. The high-pressure CO_2 cylinder, which is directly connected to the core holder by a line, was used to store CO_2, and the pressure of the

Table 1 Physical characteristics of the samples

Sample	Porosity, %	Permeability, mD	TOC content, %	Pore volume per mass, cm^3/g	Specific surface area, m^2/g	Average pore diameter, nm
Shale 1	9.6	0.012	4.62	0.0061	1.370	21.351
Shale 2	3.8	0.00053	5.20	0.0048	1.002	25.615
Sandstone 1	8.9	0.018	–	0.011647	2.6089	15.795
Sandstone 2	4.3	0.00025	–	0.004643	1.0224	18.302

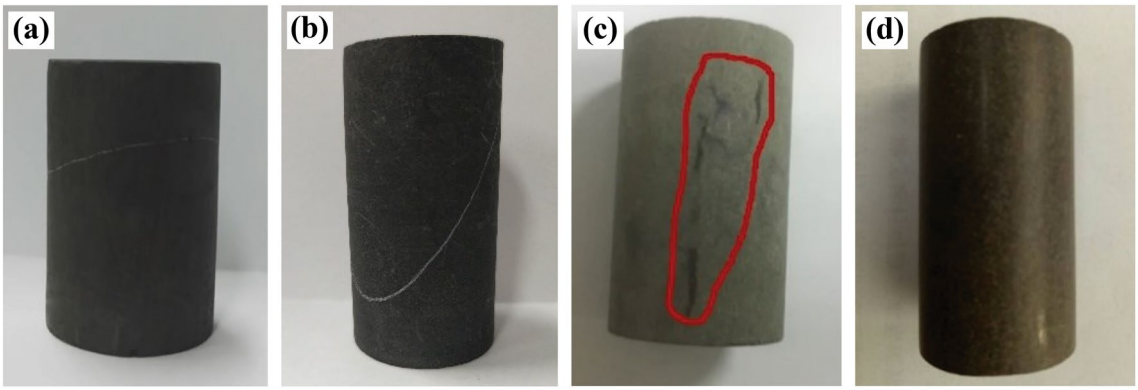

Fig. 1 Photos of the experimental cores: **a** Shale 1, **b** Shale 2, **c** Sandstone 1, **d** Sandstone 2

Table 3 Mineral compositions of the samples

Sample	Mineral composition, %									
	Quartz	Plagioclase	Potash feldspar	Dolomite	Calcite	Siderite	Pyrite	Analcite	Ankerite	Clay
Shale 1	35.2	0	0	0	1.4	0.9	7.8	35.5	19.2	0
Shale 2	27.7	8.2	0	5.5	0	1.3	6.1	0	0	51.2
Sandstone 1	41.1	28.1	10.9	13.5	0	0	0	0	0	0
Sandstone 2	64.1	10.4	7.5	11.8	3.5	0	0	0	2.7	0

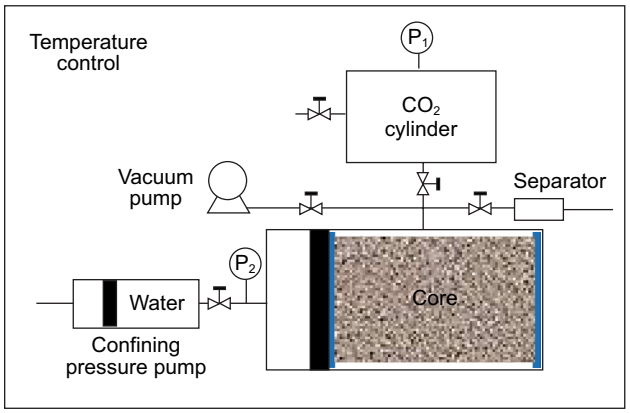

Fig. 2 Schematic of the CO_2 huff-n-puff measurement system

CO_2 cylinder was recorded by a pressure transducer. The CO_2 injection amount in the core can be obtained by the pressure decay of the CO_2 cylinder during the test. Because the volume of CO_2 has an important effect on the pressure change, 20 cm^3 was chosen as the volume of the CO_2 cylinder. If the volume of the CO_2 cylinder is larger than 20 cm^3, the pressure change will be too small to test. If the volume of the CO_2 cylinder is smaller than 20 cm^3, a large change of pressure will affect the super-critical state of CO_2. The experimental set-up was placed in an oven.

The experimental procedures are as follows.

(1) Matrix is saturated with fluid: the fractures and matrix were saturated with C_{12}, separately, to obtain the recoveries from the fracture and matrix. First, the core sample, which had been flushed for 15 days, was vacuumed for 40 h. Then, the core sample was saturated with C_{12} for 10 days at 20 MPa until their mass did not change. The mass change of the core sample was the saturated mass of C_{12} in the matrix.

(2) Fracture is saturated with fluid: the saturated core was set into the hydrostatic high-pressure core holder and held at the confining pressure, which was 2 MPa larger than the CO_2 injection pressure (pressure of CO_2 cylinder). The fracture and pressure lines were then vacuumed for 5 min to drain the gas from the fractures and pressure lines. Then, C_{12} was injected into the annulus space. The mass of C_{12}, which has been injected into the fractures, was obtained by a balance.

(3) CO_2 huff: CO_2 in the cylinder was injected into the core holder. Simultaneously, the pressure transducer was used to record the pressure of the gas cylinder.

(4) CO_2 puff: After 40 h (except Sect. 3.3, the injection times of CO_2 in Sect. 3.3 are 2, 10, 20, 40, and 60 h), the CO_2 and C_{12} mixtures in the set-up were released to the separator. The final pressure of the reservoir

decreased to zero during this step. The flashed fluid was collected during CO_2 flowing through the separator. The mass of C_{12}, which was produced during CO_2 puff, was obtained by the mass change of the separator.

(5) Steps (3) and (4) were repeated at the same initial pressure to test the recovery factor for the multicycle CO_2 huff and puff.

(6) Finally, the core was taken out of the core holder after the test and the mass change of the sample was measured.

All of the tests were performed at 60 °C, which was constant during the tests. All of the mass was tested by a high precision electronic balance with a high precision of 0.001 g. The pressure of the CO_2 cylinder was tested by a high precision pressure transducer with a precision of 0.02 MPa. The injection amount of CO_2 in the matrix–fracture system was calculated from the pressure change of the high-pressure CO_2 cylinder.

2.3 Calculation of the recovery factor and injection amount of CO_2

Fractures in reservoirs are complex, irregular, and varying; therefore, it is difficult to determine the oil recovery from the matrix and fractures using experimental methods. In this study, a simplified physical model was used to describe CO_2 huff-n-puff process, as shown in Fig. 3. The model is composed of an annular fracture and a cylindrical matrix.

As shown in Fig. 3, CO_2 initially diffuses into the fracture first and then into the matrix during the CO_2 huff process. During the CO_2 puff process, the CO_2 and C_{12} mixtures are released first from the fracture and then from the matrix. There is little oil in the CO_2 cylinder after the experiment. Therefore, it is reasonable to assume that the oil components, which diffuse from the core into the CO_2 cylinder, are negligible during CO_2 huff-n-puff. The oil production (mass) after nth cycle CO_2 huff-n-puff is obtained by the mass of C_{12} collected by the separator of the nth cycle. The oil production (mass) of the matrix is obtained by the mass change of the core after the experiment. The oil production (mass) of fracture is obtained by the difference between the total oil production and oil production of the matrix after the experiment. The incremental recovery factor of original oil-in-place (OOIP) after nth cycle, the matrix recovery factor of OOIP, and the fracture recovery factor of OOIP can be calculated from the following equations:

$$\begin{cases} \eta^n = \dfrac{\sum_1^n m_s^n}{m_{m0} + m_f}, \quad n = 1, 2, 3 \cdots \\ \eta_m = \dfrac{m_{m0} - m_{m1}}{m_{m0}} \\ \eta_f = \dfrac{m_s - (m_{m0} - m_{m1})}{m_f} \end{cases} \tag{1}$$

where η^n is the incremental recovery factor of OOIP after nth cycles; η_m is the matrix recovery factor of OOIP at the end of the experiment; η_f is the fracture recovery factor of OOIP at the end of the experiment; m_{m0} is the total mass of C_{12} in the matrix, g; m_f is the total mass of C_{12} in the fracture, g; m_s^n is the mass of C_{12} collected by the separator of the nth cycle, g; m_s is the total mass of C_{12} collected by the separator at the end of the experiment, g; and m_{m1} is the mass of C_{12} in the matrix at the end of the experiment, g.

The CO_2 injectivity in the samples is positively correlated with the injection amount of CO_2 into the matrix–fracture system (Δn_{CO_2}), which is a key factor in the recovery factor during CO_2 huff-n-puff and can be calculated by Eq. (2).

$$\Delta n_{CO_2} = \frac{n_0 - n_t}{V_m} = \left(\frac{p_0 v}{z_0 RT} - \frac{p_t v}{z_t RT} \right) \frac{1}{V_m} \tag{2}$$

where Δn_{CO_2} is the injection amount of CO_2 during the test, which is the amount of CO_2 injected per volume of the matrix–fracture system, mol/cm^3; n_0 is the initial amount of CO_2 in the CO_2 cylinder, mol; n_t is the remaining CO_2 in the CO_2 cylinder, mol; V_m is the volume of the matrix–fracture system, cm^3; p_0 is the initial pressure of the CO_2 cylinder, MPa; z_0 is the compressibility factor at p_0; p_t is the pressure of the CO_2, MPa; z_t is the compressibility factor of CO_2 at p_t; v is the CO_2 cylinder volume, cm^3; R is the Avogadro constant, $R = 8.314$ J/(mol K); and T is the experimental temperature, K.

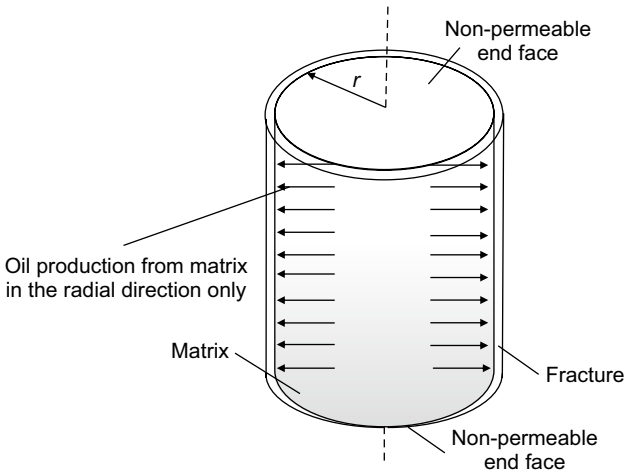

Fig. 3 Schematic of oil production during CO_2 huff-n-puff

3 Results and discussion

3.1 Effect of rock properties

The incremental recovery factors in Shale 1, Shale 2, Sandstone 1, and Sandstone 2 after three cycles of CO_2 injection were tested at 20 MPa and 60 °C. As shown in Table 1, the porosity of Shale 1 (9.6%) was close to Sandstone 1 (8.9%) and the porosity of Shale 2 (3.8%) was close to Sandstone 4 (4.3%). Figure 4 shows the pore size distributions of the four samples, which is tested by liquid nitrogen adsorption measurements. The pore volume of Sandstone 1 was larger than other samples. According to Table 1, the porosity of Shale 1 was similar to Sandstone 1. However, the incremental pore volume of Shale 1 was far less than that of Sandstone 1. The reason was that the porosity in Table 1 was tested by the saturation of C_{12} and the incremental pore volume in Fig. 4 was tested by nitrogen. Because C_{12} can dissolve in the kerogen, which is inaccessible for nitrogen, the incremental pore volume of Shale 1 in Fig. 1 was less than that of Sandstone 1. Besides, the results of Fig. 4 indicated that Shale 1 had a greater degree of micropores (with widths smaller than 2 nm) than the other samples. The incremental recovery factor, matrix recovery factor, and fracture recovery factor were obtained by Eq. (1) for the four samples after three cycles of CO_2 huff-n-puff.

Figure 5 shows the incremental recovery factors from different samples after three cyclic injections of CO_2. The results show that η^n increased with porosity after the same cycle for the shale and sandstone. Moreover, the incremental recovery factors of Sandstone 1 and 2 werte greater than those of Shale 1 and 2, respectively. The reason was that there was a larger amount of adsorption–dissolution C_{12} in the kerogen, which was hard to be mobilized during CO_2 injection. Moreover, the increasing rate of the incremental recovery factor of sandstone decreased more rapidly with the number of cycles than shale, especially for the samples with low porosity. It has been reported that the adsorption-dissolution C_{12} in the kerogen was only replaced by CO_2 when the concentration of CO_2 was large enough (Zhu et al. 2018b). Because the amount of C_{12} in the shale decreased with the number of cycles, the concentration of CO_2 in the matrix also increased with the number of cycles. Therefore, the production decline in the shale was smaller than that in the sandstone, and more cycles are needed during CO_2 huff-n-puff process for shale to reach a larger recovery factor.

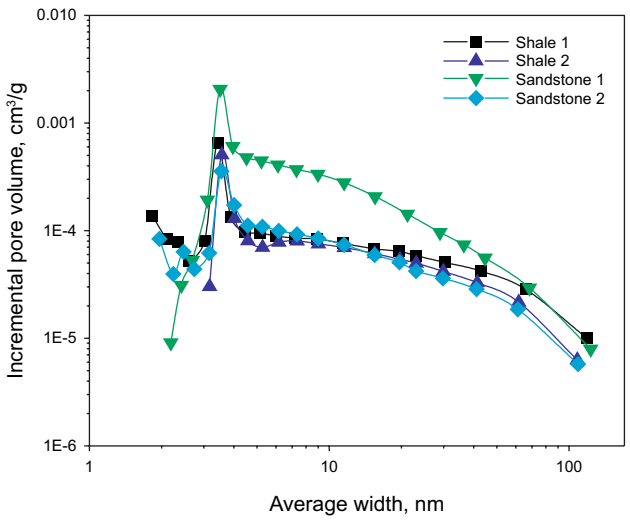

Fig. 4 Pore size distributions of the samples

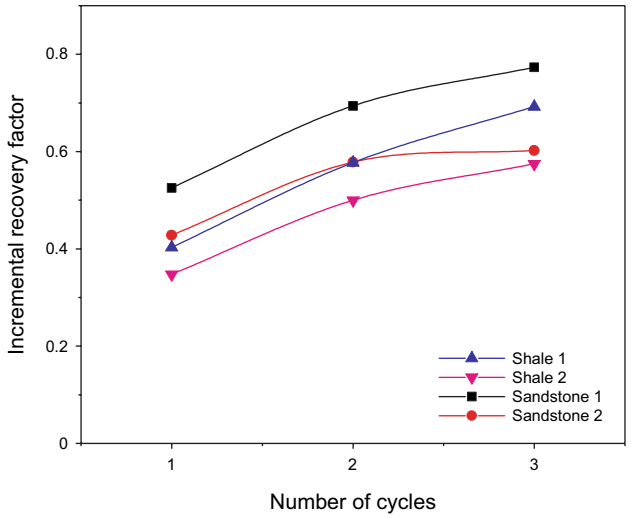

Fig. 5 Incremental recovery factors of different core samples during the CO_2 huff-n-puff process (20 MPa, 60 °C)

Figure 6 shows the relationships between Δn_{CO_2} and time in the matrix–fracture systems of the four samples, which can be calculated by the CO_2 pressure decline curves in Fig. 15 in "Appendix," and Table 4 shows the values of Δn_{CO_2}, $\Delta n^1_{CO_2}$, and $\Delta n^2_{CO_2}$ during three cycles for the different samples. In the first cycle, because the samples were completely saturated with C_{12}, CO_2 diffused into oil and adsorbed in the kerogen with time. However, Δn_{CO_2} curves can be divided into two stages in the second and third cycles. In the first stage, a mass of CO_2 ($\Delta n^1_{CO_2}$) enters into the matrix–fracture system quickly at the beginning. The reason was that there is an empty matrix–fracture space after oil produced from the system during the first and second cycle puffs. The empty matrix–fracture space should be filled by CO_2 first in the second and third cycles. In the second stage, CO_2 was injected slowly into the matrix–fracture system ($\Delta n^2_{CO_2}$), which diffused into oil and adsorbed in the kerogen. Because the empty matrix–fracture space after the CO_2 puff increased with the number of cycles, $\Delta n^1_{CO_2}$ also increased

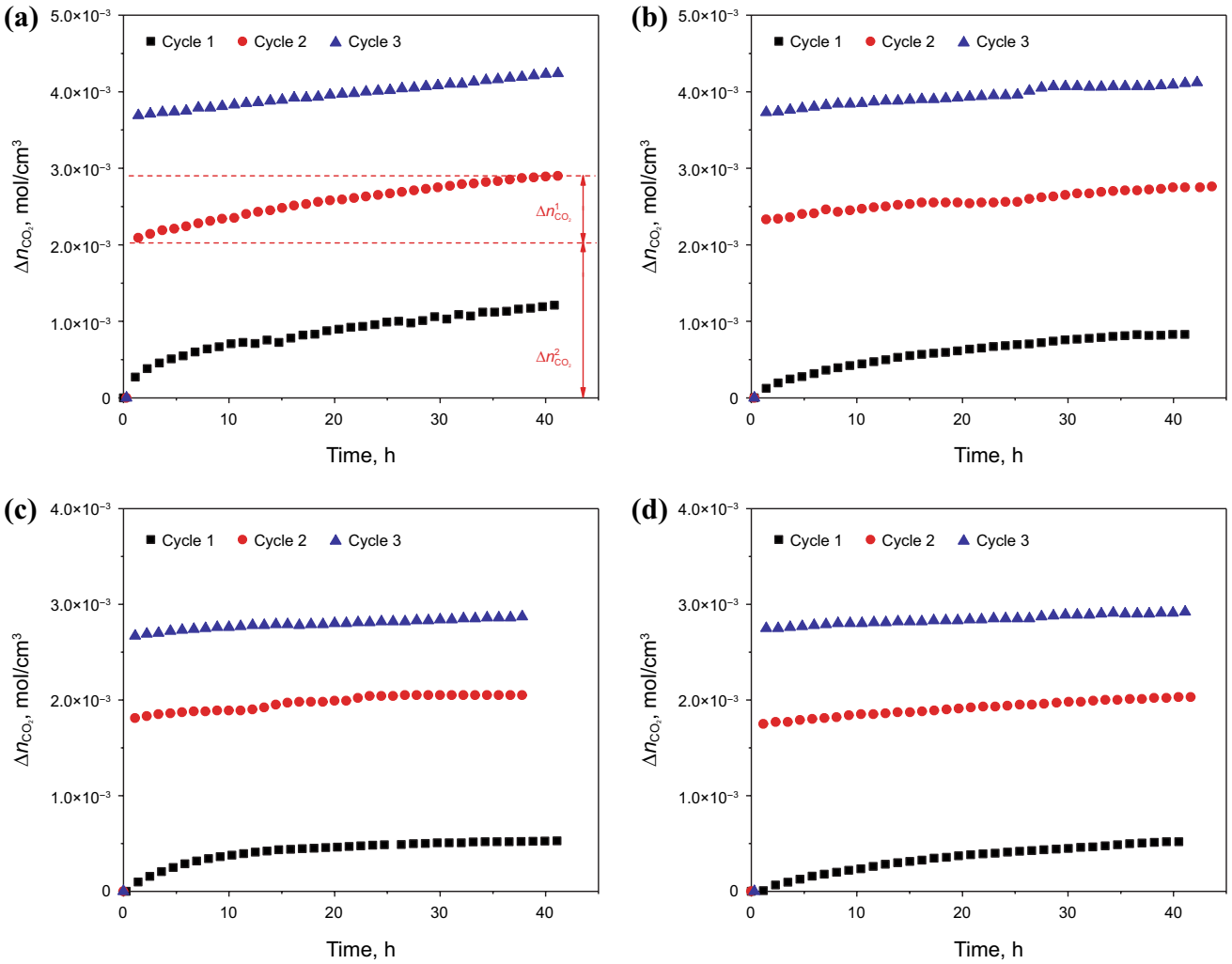

Fig. 6 Relationships between Δn_{CO_2} and time for four samples: **a** Shale 1; **b** Sandstone 1; **c** Shale 2; **d** Sandstone 2

Table 4 Values of Δn_{CO_2}, $\Delta n^1_{CO_2}$, and $\Delta n^2_{CO_2}$ during three cycles in the different samples

Sample	Porosity, %	Number of cycles	Δn_{CO_2}, 10^{-3} mol/cm^3	$\Delta n^1_{CO_2}$, 10^{-3} mol/cm^3	$\Delta n^2_{CO_2}$, 10^{-3} mol/cm^3
Shale 1	9.6	1	1.22	0.00	1.22
		2	2.96	2.10	0.86
		3	4.26	3.70	0.56
Shale 2	3.8	1	0.53	0.00	0.53
		2	2.05	1.79	0.26
		3	2.97	2.74	0.23
Sandstone 1	8.9	1	0.82	0.00	0.82
		2	2.76	2.34	0.42
		3	4.13	3.73	0.40
Sandstone 2	4.3	1	0.52	0.00	0.52
		2	2.03	1.77	0.27
		3	2.92	2.75	0.17

with the number of cycles. Moreover, the increasing rates of $\Delta n^2_{CO_2}$ with time in the first cycle were greater than the others. The reason was that the amount of C_{12} in the shale after the CO_2 puff decreased with the number of cycles increasing.

As shown in Fig. 6 and Table 4, $\Delta n^1_{CO_2}$ of Shale 1 in different cycles were larger than those of Shale 2, and $\Delta n^1_{CO_2}$ of Sandstone 1 were larger than those of Sandstone 2. Because the porosity of Shale 1 (9.6%) and Sandstone 1 (8.9%) was higher than those of Shale 2 (3.8%) and Sandstone 2 (4.3%), more CO_2 was needed to fill the empty matrix–fracture space in Shale 1 and Sandstone 1 during the second and third cycles. Therefore, $\Delta n^1_{CO_2}$ increased with increasing porosity. $\Delta n^2_{CO_2}$ of Shale 1 during the three cycles of CO_2 injection were 1.22×10^{-3}, 0.86×10^{-3} and 0.56×10^{-3} mol/cm^3, respectively, which were larger than those of Sandstone 1 (0.82×10^{-3}, 0.42×10^{-3} and 0.40×10^{-3} mol/cm^3). Because

Table 5 Values of η^n, η_m, and η_f of the samples after three cycles of CO_2 injection

Sample	m_{m0}, g	m_f, g	η^n, %	η_m, %	η_f, %
Shale 1	1.371	1.220	69.2	50.5	82.2
Shale 2	0.934	2.650	57.4	18.5	72.3
Sandstone 1	1.280	1.422	77.3	74.3	80.5
Sandstone 2	0.955	1.731	60.2	31.2	70.6

CO_2 was adsorbed and dissolved in the kerogen during cyclic CO_2 injection, the $\Delta n^2_{CO_2}$ of the shale was larger than that of sandstone when the porosity was similar. The relationships between $\Delta n^2_{CO_2}$ and the number of cycles for Shale 2 and Sandstone 2 were similar to those of Shale 1 and Sandstone 1.

As shown in Table 5, the incremental recovery factor (η^n), matrix recovery factor (η_m), and fracture recovery factor (η_f) for different samples after three cycles of CO_2 injection were obtained by Eq. (1). η_m and η_f both increased with porosity for the same rock properties. Although the porosities of Shale 1 and Sandstone 1 were approximately the same, η_m of Shale 1 (50.5%) was less than that of Sandstone 1 (74.3%) after three cycles of CO_2 injection. Besides, η_m of Shale 2 (18.5%) was smaller than that of Sandstone 2 (31.2%). Prat of oil in the shale was adsorbed and dissolved in the kerogen, which was hard to be replaced by CO_2. Therefore, η_m of shale was always smaller than that of sandstone when the porosities were approximately the same. η_f of Shale 1 (82.2%) was slightly greater than that of Sandstone 1 (80.5%), and η_f of Shale 2 (72.3%) was slightly greater than that of Sandstone 2 (70.6%). Because the size of the fracture was only 1 mm, the diffusion length of CO_2 in the fracture was far less than that in the matrix. According to Fick's law, the equilibrium time of CO_2 in the fracture was short (0.5 h), which was far less than 40 h (test time). CO_2 was saturated in the fracture under different injection pressures during the test. Therefore, the concentration of CO_2 in the fracture was similar in the shale and sandstone. However, $\Delta n^2_{CO_2}$ of the shales were slightly larger than those of the sandstones because of the adsorption and dissolution of CO_2 in the kerogen (Table 4). Therefore, more CO_2 flowed through the fracture during the CO_2 puff and the displacement efficiencies of fractures in the shales were slightly better than those in the sandstones when the porosities of them was similar. Besides, η_f increased with increasing porosity when the rock properties were the same. The reason for this result was similar to that described above. Because more CO_2 was injected into the higher-porosity matrix during the CO_2 huff, more CO_2 flowed through the fracture during the CO_2 puff. Therefore, the displacement efficiency of fracture with a higher porosity matrix was better.

As shown in Table 4, although $\Delta n^1_{CO_2} > \Delta n^2_{CO_2}$ in the second and third cycles, the contributions of $\Delta n^2_{CO_2}$ to the recovery factors were higher than $\Delta n^1_{CO_2}$. However, because empty matrix–fracture space should be filled with CO_2 at the second and third cycles, $\Delta n^1_{CO_2}$ was necessary during CO_2 huff-n-puff.

3.2 Effect of injection pressure

The recovery factor after three cyclic injections of CO_2 in Shale 1 was tested at 60 °C and different operating pressures (6, 9, 12, 15, and 20 MPa). According to the test, m_{m0} and m_f were 1.371 and 1.220 g, respectively. Moreover, the volumes of fracture and matrix were 1.691 and 18.064 cm^3, respectively. Figure 7 shows the relationship between recovery factors in Shale 1 and the operating pressure during CO_2 huff-n-puff process.

According to Eq. (1), the incremental recovery factor (η^n), the matrix recovery factor (η_m), and the fracture recovery factor (η_f) were obtained at different pressures after three cycles of CO_2 injections. As shown in Fig. 7, η_m increased from 28.3% to 50.5%, and η_f increased from 68.5% to 82.3% when the injection pressure of CO_2 moved from 6 to 20 MPa. Moreover, the increasing rates of η_m and η_f with pressure were different. η_m increased dramatically from approximately 31.8% to 49.8% when the pressure moved from 9 to 15 MPa, whereas η_m only increased by 0.7% when the pressure moved from 15 to 20 MPa. The MMP of the C_{12} and CO_2 mixture was 13.8 MPa at 60 °C (Zhu et al. 2018b, c). However, η_f did not increase significantly when the pressure neared the MMP (9–15 MPa) because the diffusion coefficient and boundary concentration of CO_2 both

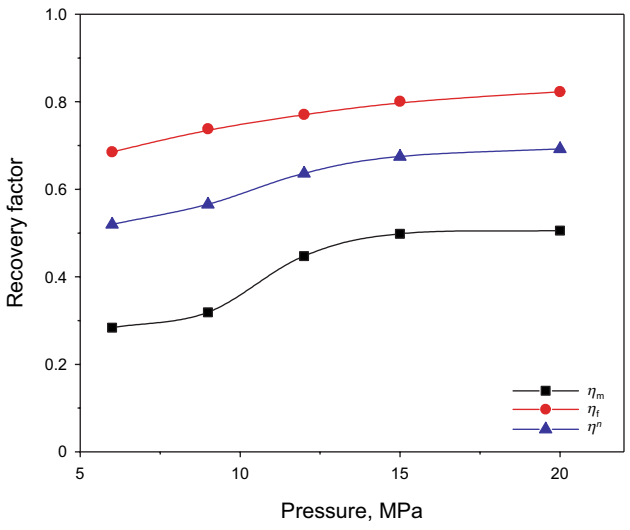

Fig. 7 Relationship between recovery factors in Shale 1 and the operating pressure during CO_2 huff-n-puff process

increased with pressure (Li et al. 2016). Thus, the flux of CO_2 that diffused into the matrix increased sharply when the pressure neared the MMP. Therefore, the matrix recovery factor increased drastically. However, for the CO_2 flux in the fracture, the influence of the diffusion coefficient could be negligible because the diffusion length of CO_2 in the fracture was far less than that in the matrix. On the contrary, the amount of CO_2 flow from the matrix to the fracture and the concentration of CO_2 in the fracture increased pressure. Therefore, although η_f increased with pressure, the increasing rate of η_f did not increase significantly when the pressure neared the MMP.

Figure 8 is the incremental recovery factor in Shale 1 at different operating pressures, which shows that the incremental recovery factors (η^n) all increased with the injection pressure for the same cycle. Regardless of whether the injection pressure was at immiscible or miscible conditions, the recovery factor of the first cycle was more than double that of the second cycle and the greatest contribution to the incremental recovery factor (more than 50%) came from the first cycle.

Figure 9 shows the relationships between Δn_{CO_2} and time at different injection pressures, which were calculated by the CO_2 pressure decline curves in Fig. 17 in "Appendix". Therefore, $\Delta n^1_{CO_2}$ and $\Delta n^2_{CO_2}$ at different pressures could be obtained. Figure 10 shows the relationships between the injection amount of CO_2 and pressure in Shale 1 during three cycles of CO_2 injection. As shown in Fig. 10a, $\Delta n^1_{CO_2}$ increased with the injection pressure for the same cycle. There are two reasons for this phenomenon: (1) Because the incremental recovery factor increased with pressure (Fig. 8), the empty matrix–fracture space increased with pressure after the same cycle. The empty matrix–fracture space should be filled with CO_2 first. Therefore, $\Delta n^1_{CO_2}$ increased with the injection pressure for the same cycle. (2) The density of CO_2 also increased with pressure. As shown in Fig. 10b, $\Delta n^2_{CO_2}$ initially increased with pressure and the increasing rate of $\Delta n^2_{CO_2}$ reduced rapidly when the pressure was higher than 12 MPa. The adsorption-dissolution amount of CO_2 in the kerogen and the diffusion coefficient of CO_2 in C_{12} both increased with the injection pressure, which had an important effect on $\Delta n^2_{CO_2}$ (Li et al. 2016; Zhu et al. 2018b). Therefore, $\Delta n^2_{CO_2}$ increased with the injection pressure. However, the diffusion coefficient of CO_2 in C_{12} remained nearly constant when the pressure was higher than the MMP (13.8 MPa). Therefore, the increasing rate of $\Delta n^2_{CO_2}$ reduced rapidly when the pressure was higher than 12 MPa.

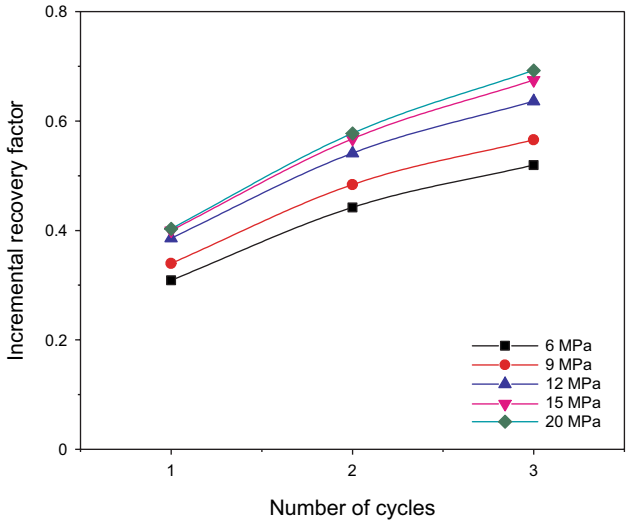

Fig. 8 Incremental recovery factor in Shale 1 at different operating pressures

Next, the relationships between recovery factor and Δn_{CO_2} in Shale 1 during three cycles of CO_2 injection were studied. However, because the residual oil-in-place of the second and third cycles is different from the first cycle, the incremental recovery factor of OOIP in the second and third cycles was less than that in the first cycle. Therefore, the recovery factor of residual oil-in-place (ROIP) at the nth cycle was calculated by Eq. (3).

$$\eta^n_{re} = \frac{m^n_s}{m_{m0} + m_f - \sum m^{n-1}_s}, \quad n = 1,\ 2,\ 3\ldots \tag{3}$$

where η^n_{re} is the recovery factor of ROIP at the nth cycle.

Figure 11 shows the relationships between η^n_{re} and Δn_{CO_2} in Shale 1. The results show that η^n_{re} in different cycles increased linearly with the injection amount of CO_2. Although Δn_{CO_2} in the first cycle was smaller than that in the second and third cycles, η^n_{re} in the first cycle was larger than that in the second and third cycles. The reason was that part of the CO_2 was injected into the empty matrix–fracture space during the second and third cycles, which had no contribution to the recovery factor. The results indicate that η^n_{re} in the first cycle is the largest contributor to the recovery factor. Moreover, when the pressure was higher than the MMP, the increasing of η^n_{re} and Δn_{CO_2} in the first cycle were both small. The reason is that the change of diffusion coefficient and boundary concentration of CO_2 in the shale were small when the pressure was higher than the MMP. Because the injection amount and pressure of CO_2, which both changed with pressure during CO_2 huff-n-puff, had a combined effect on the results in Fig. 11, the effect of injection time on the recovery factor was studied in the next section (which had the same pressure and different injection amount of CO_2).

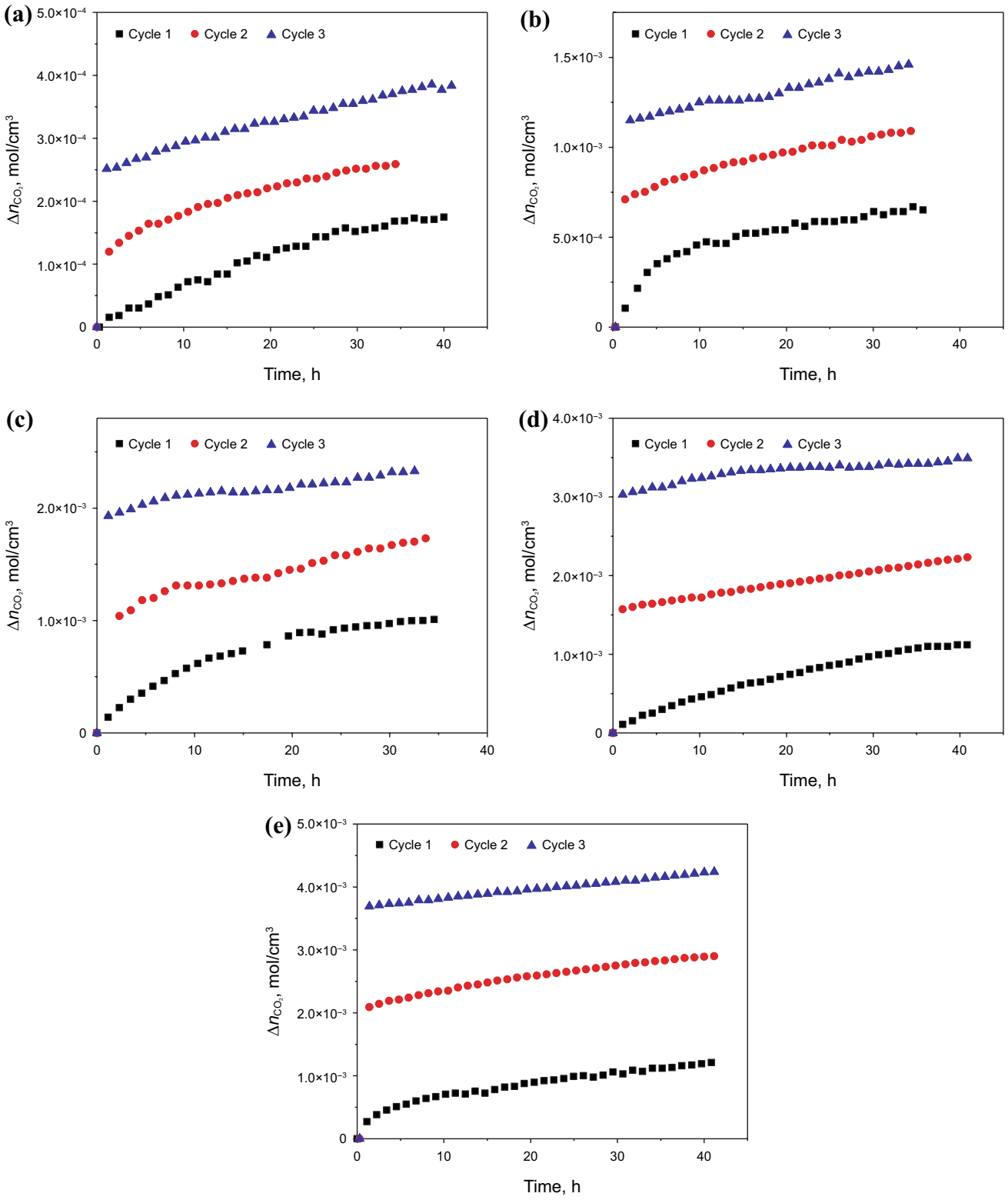

Fig. 9 Relationships between Δn_{CO_2} and time at different injection pressures: **a** 6 MPa; **b** 9 MPa; **c** 12 MPa; **d** 15 MPa; **e** 20 MPa

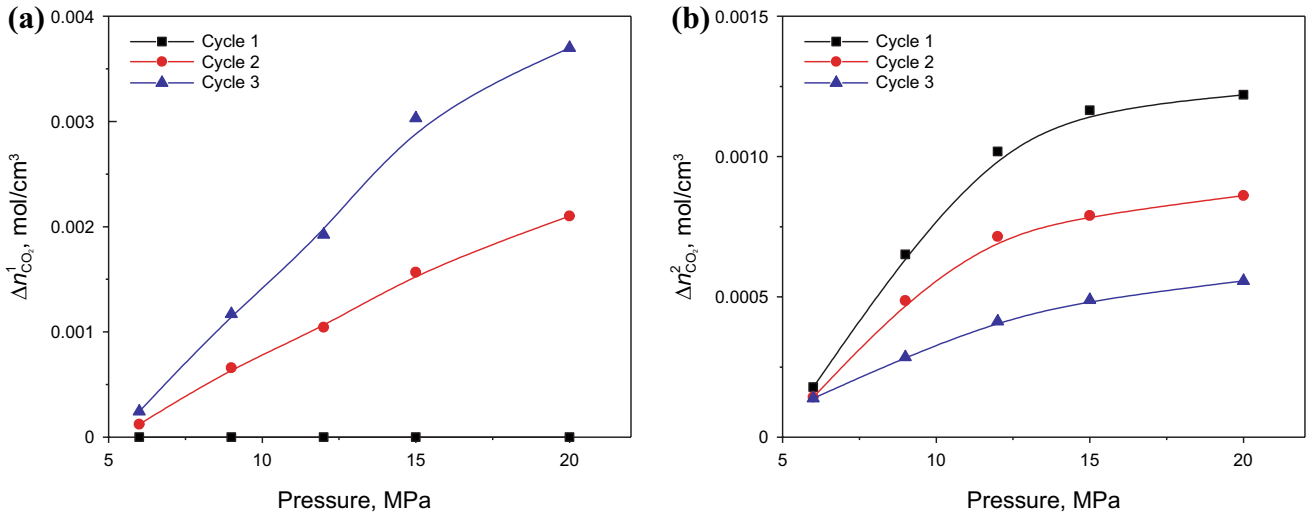

Fig. 10 Relationships between the injection amount of CO_2 and pressure during three cycles CO_2 huff-n-puff: **a** $\Delta n^1_{CO_2}$; **b** $\Delta n^2_{CO_2}$

3.3 Effect of injection time

The recovery factors in Shale 1 and Sandstone 1 after one cycle of CO_2 injection were determined at different injection times (2, 10, 20, 40, and 60 h) at 12 MPa and 60 °C. The incremental recovery factor, matrix recovery factor, and fracture recovery factor were calculated using Eq. (1).

Figure 12 shows the recovery factors in Shale 1 and Sandstone 1 at different injection times. The results show that an increase in injection time from 2 to 60 h amounts to a 13.2% (25.7%–38.9%) increase in η^n. As shown in Fig. 12b, η^n of Sandstone 1 increased from 26.6% to 46.4%, which was a slightly greater increase than that in Shale 1. The recovery factor consists of two components, the fracture recovery factor and the matrix recovery factor, which will be explained below.

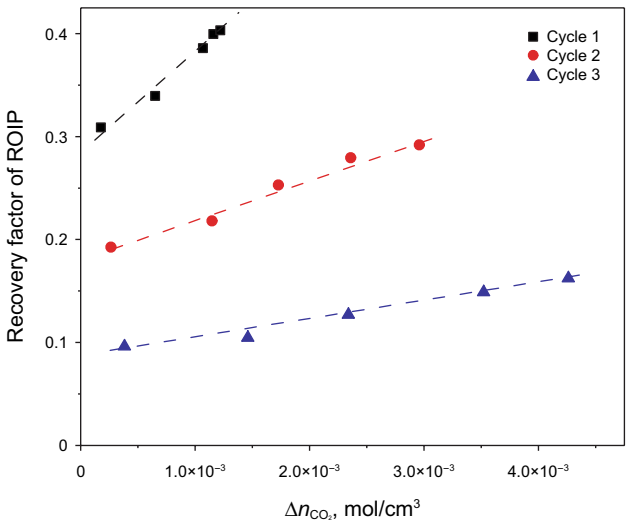

Fig. 11 Relationships between recovery factor of ROIP at the *n*th cycle (η^n_{re}) and Δn_{CO_2}

First, when the injection time increased from 2 to 60 h, η_f of Shale 1 increased from 39.2% to 46.2% and η_f of Sandstone 1 increased from 39.9% to 49.4%. As the injection time increased, more CO_2 was injected into the matrix during the CO_2 huff; therefore, a larger amount of CO_2 flowed from the matrix through the fracture during the CO_2 puff. The displacement efficiency of the fracture was better for a long injection time during the CO_2 puff. Moreover, η_f of Shale 1 was slightly larger than that of Sandstone 1 for the same injection time. The reason was that the injection amount of CO_2 in the matrix of Shale 1 was slightly larger than that in Sandstone 1 because of the adsorption-dissolution of CO_2 in the kerogen. According to our previous research, the adsorption amount of CO_2 in the shale can reach 0.92–2.58 mmol/g, which depends on the TOC (Zhu et al. 2019). The displacement efficiency of the fracture in Shale 1 was better than that in Sandstone 1 during the CO_2 puff. Therefore, the η_f of Shale 1 was slightly greater than that of Sandstone 1 for the same injection time.

Second, when the injection time increased from 2 to 60 h, η_m of Shale 1 increased from 9.0% to 28.7% and η_m of Sandstone 1 increased from 14.0% to 43.2%. Because the injection pressure and temperature were the same in this section, the diffusion coefficient and boundary concentration of CO_2 in C_{12} were the same. The flux of CO_2, which diffused into the matrix, increased with injection time. Therefore, the matrix recovery factor increased with the injection time. It should be noted that the injection time had a greater effect on the matrix recovery factor than on the fracture recovery factor. This result occurred because the diffusive equilibrium time of CO_2 in the matrix was much longer than that in the fracture (0.5 h). The effect of the injection time on the

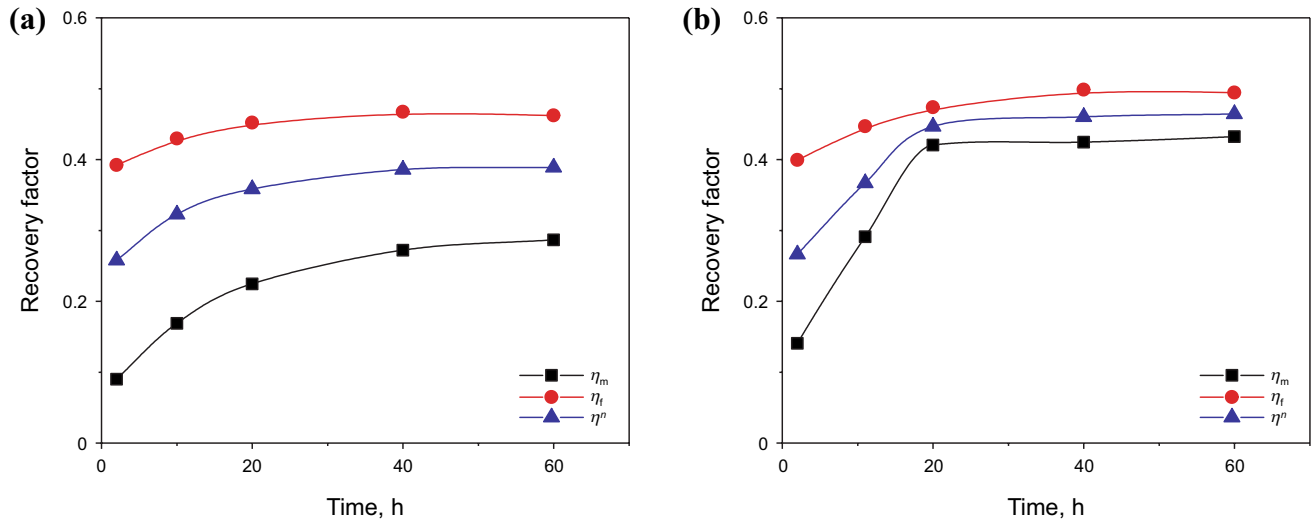

Fig. 12 Recovery factors of the CO_2 huff-n-puff process for different injection times: **a** Shale 1; **b** Sandstone 1

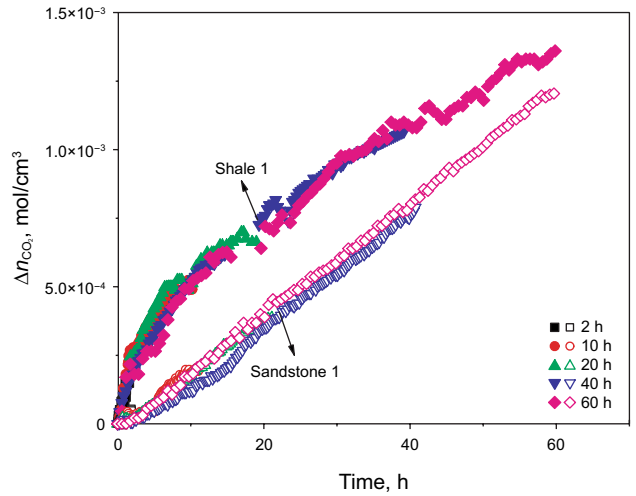

Fig. 13 Relationships between Δn_{CO_2} and time for Shale 1 and Sandstone 1 at 12 MPa and 60 °C

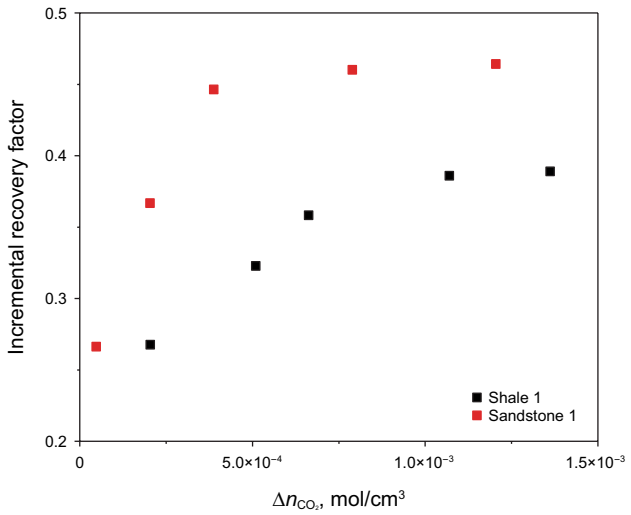

Fig. 14 Relationships between the recovery factor and Δn_{CO_2} at 12 MPa and 60 °C

fracture was small during the CO_2 cycle injection. Moreover, η_m of the sandstone was greater than that of shale for different injection times. The reason for this was that part of the oil in the shale was adsorbed and dissolved in the kerogen, which was difficult to be produced.

Furthermore, η_m of Sandstone 1 did not increase with the injection time when the injection time was longer than 20 h. However, η_m of Shale 1 kept increasing with increasing injection time during the test. Therefore, more injection time is required for shale to reach the maximum recovery factor.

The injection amount of CO_2 (Δn_{CO_2}) in the matrix–fracture systems for different injection times were calculated by Eq. (2) (Fig. 13), which can be calculated by the CO_2 pressure decline curves in Fig. 17 in "Appendix". The Δn_{CO_2} curves for different injection times were the same for the same samples. The growth rate of Δn_{CO_2} in Shale 1 was larger than that in Sandstone 1, especially at the beginning. There were two reasons: (1) There were layers and microfractures in the shale, which was beneficial to CO_2 diffusion at the beginning. (2) A larger amount of CO_2 was adsorbed

and dissolved into the kerogen to replace the adsorption–dissolution oil during CO_2 injection in the shale.

Figure 14 shows the relationships between the recovery factor and Δn_{CO_2} for Shale 1 and Sandstone 1 at 12 MPa and 60 °C, which shows that the recovery factor increased with the injection amount of CO_2. However, when Δn_{CO_2} was greater than 1.07×10^{-3} mol/cm^3 (40 h), the recovery factor of Shale 1 did not increase with Δn_{CO_2}. Similarly, the recovery factor of Sandstone 1 did not increase with Δn_{CO_2} when it was greater than 3.88×10^{-4} mol/cm^3 (20 h). The cause of this phenomenon appeared to be the collapse of foamy flow due to a higher volume of released CO_2. Because of the higher Δn_{CO_2}, more gas is released from the solution than can be dispersed during CO_2 puff; therefore, when Δn_{CO_2} is large, CO_2 flows as a continuous phase (Busahmin and Maini 2010). When Δn_{CO_2} was greater than the optimal value, the recovery factor did not increase with Δn_{CO_2}. Besides, the optimal value of Δn_{CO_2} in the shale (1.07×10^{-3} mol/cm^3, 40 h) was larger than that in the sandstone (3.88×10^{-4} mol/cm^3, 20 h). Because CO_2 can be adsorbed and dissolved in the kerogen, the critical gas saturation of shale was larger than sandstone. Therefore, a higher Δn_{CO_2} for shale was needed to form a continuous phase. These results indicate that there were optimal values of Δn_{CO_2} for CO_2 huff-n-puff and more injection time was needed for shale to reach the optimal Δn_{CO_2}.

4 Conclusions

A modified experimental method is developed to investigate the recovery factors and injectivity of CO_2 in the fracture–matrix system. The oil recovery factors of shales with different porosities are compared with sandstones to study the effects of kerogen on CO_2 huff-n-puff. The effects of rock properties, injection pressure, and injection time on the recovery factors are discussed. The major conclusions are as follows:

(1) The matrix recovery factor in Shale 1 (50.5%) and Shale 2 (18.5%) are much lower than that in Sandstone 1 (74.3%) and Sandstone 1 (31.2%) during CO_2 huff-n-puff, while the injectivity of CO_2 in the shale is larger than that in the sandstone. However, the production decline of the shale is smaller than sandstone. Therefore, more cycles are needed for the shale to reach a large recovery factor than the tight sandstone.

(2) Injection pressure has an important impact on the recovery factors of the shale. When the injection pressure increases from an immiscible pressure to a miscible pressure, the recovery factors of the shale and the injectivity of CO_2 increases dramatically during CO_2 huff-n-puff. The optimal injection pressure of CO_2 huff-n-puff in the shale is close to the MMP (13.8 MPa).

(3) The injectivity of CO_2 in the shale is better than the sandstone, especially at the beginning, because there are layers and microfractures in the shale and parts of CO_2 are adsorbed and dissolved in the kerogen. Meanwhile, there are optimal CO_2 injection amount during the huff-n-puff process, and the optimal CO_2 injection amount in the shale (1.07×10^{-3} mol/cm^3) is larger than that in the sandstone (3.88×10^{-4} mol/cm^3) at 12 MPa. Besides, more injection time is needed for the shale (40 h) to reach the optimal CO_2 injection amount than the tight sandstone (20 h).

(4) The effects of sample properties, injection pressure, and time on the fracture recovery factor are smaller than those on the matrix recovery factor because the diffusion distance and equilibrium time of CO_2 in the fracture is short. Therefore, the application of multiple refracturing with CO_2 to generate microfractures is beneficial to enhancing shale oil recovery.

Acknowledgements We gratefully acknowledge the National Key R&D Program of China (Grant No. 2019YFA0705502, Grant No. 2019YFA0705501), the financial support from the Shandong Provincial Natural Science Foundation (ZR2019QEE037, ZR2019MEE058), and the Fundamental Research Funds for the Central Universities (17CX05005, 18CX02104A).

Appendix: pressure decline curves

See Figs. 15, 16 and 17.

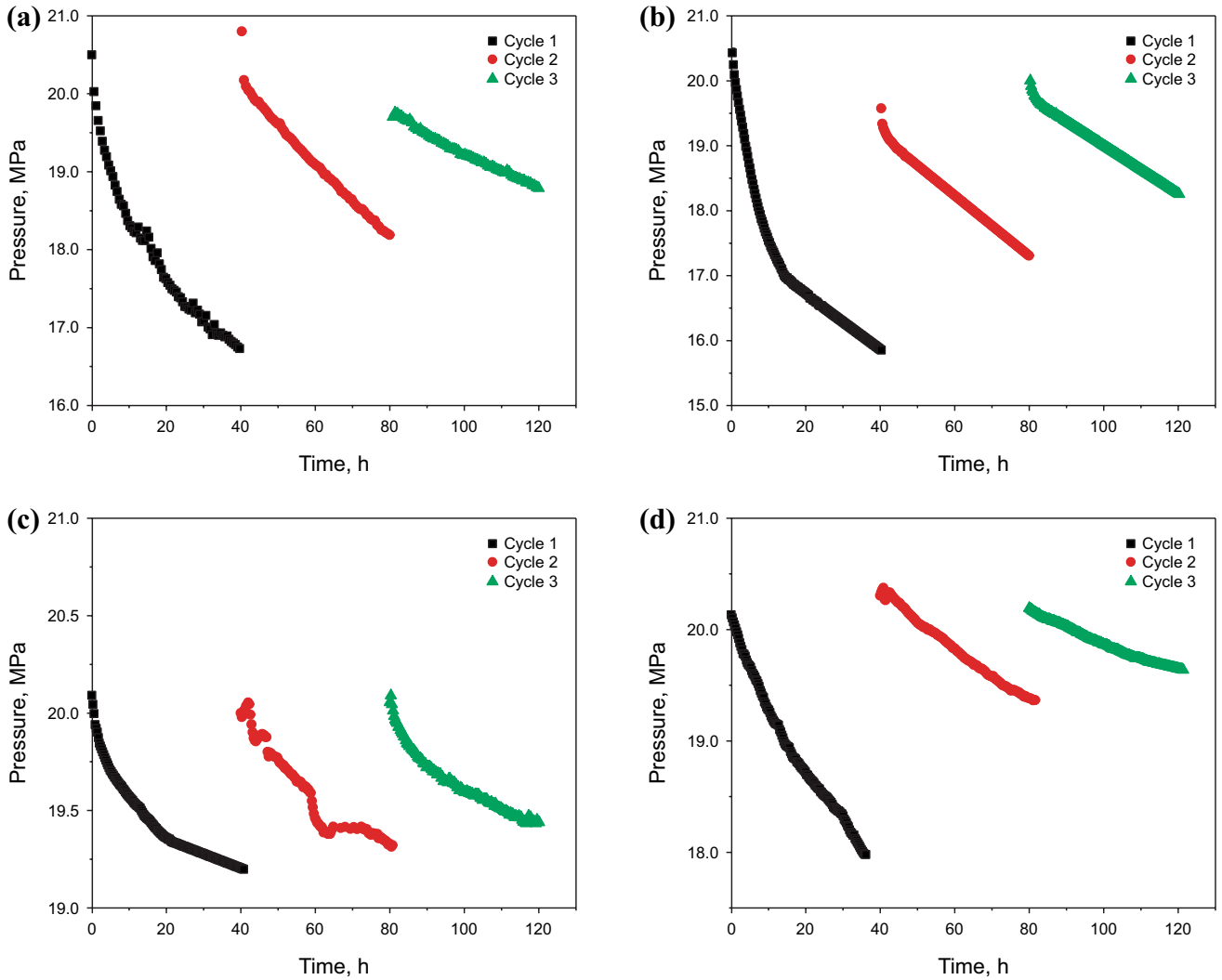

Fig. 15 Relationships between pressure and time for different samples: **a** Shale 1; **b** Sandstone 1; **c** Shale 2; **d** Sandstone 2

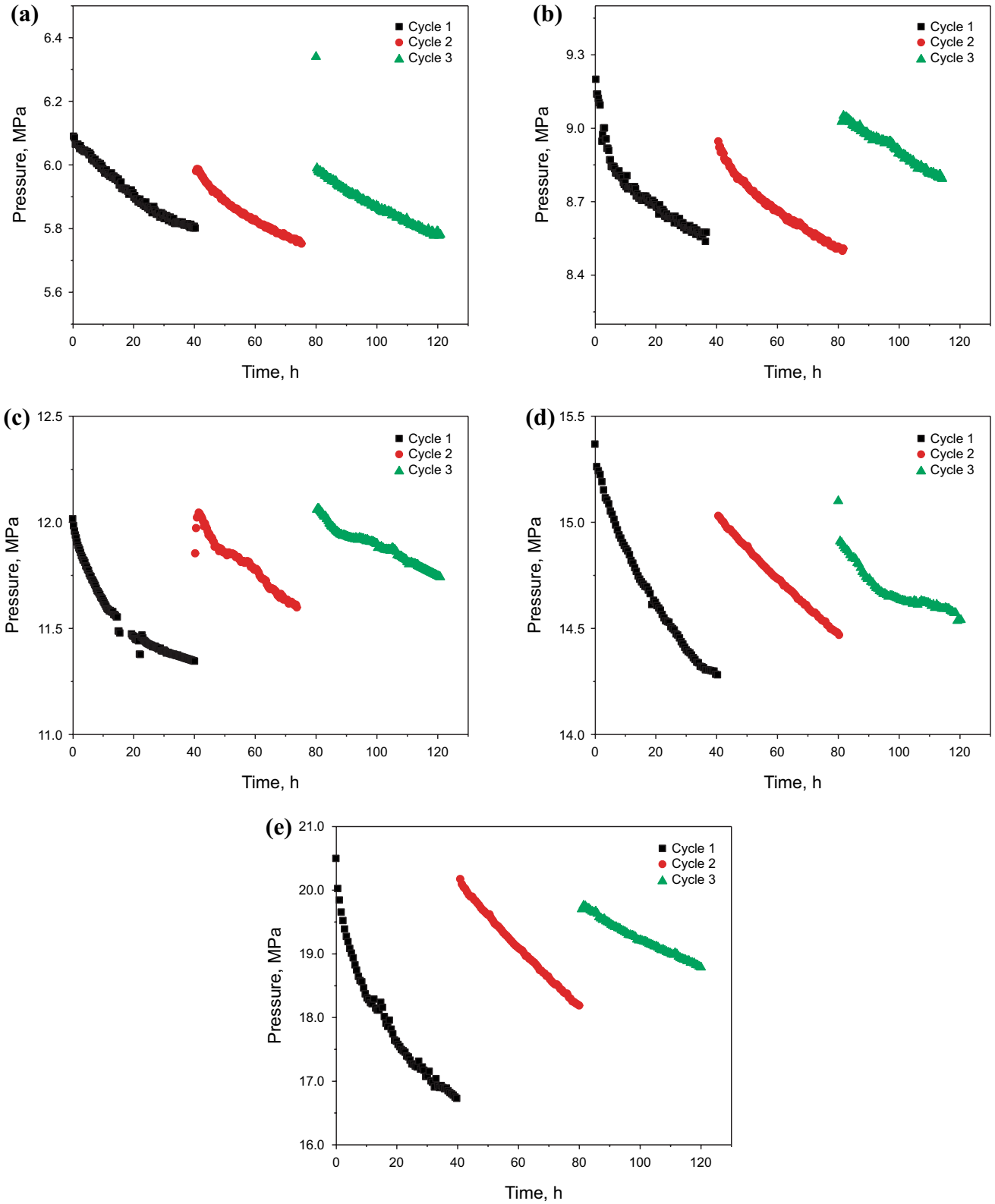

Fig. 16 Relationships between pressure and time at different injection pressures: **a** 6 MPa; **b** 9 MPa; **c** 12 MPa; **d** 15 MPa; **e** 20 MPa

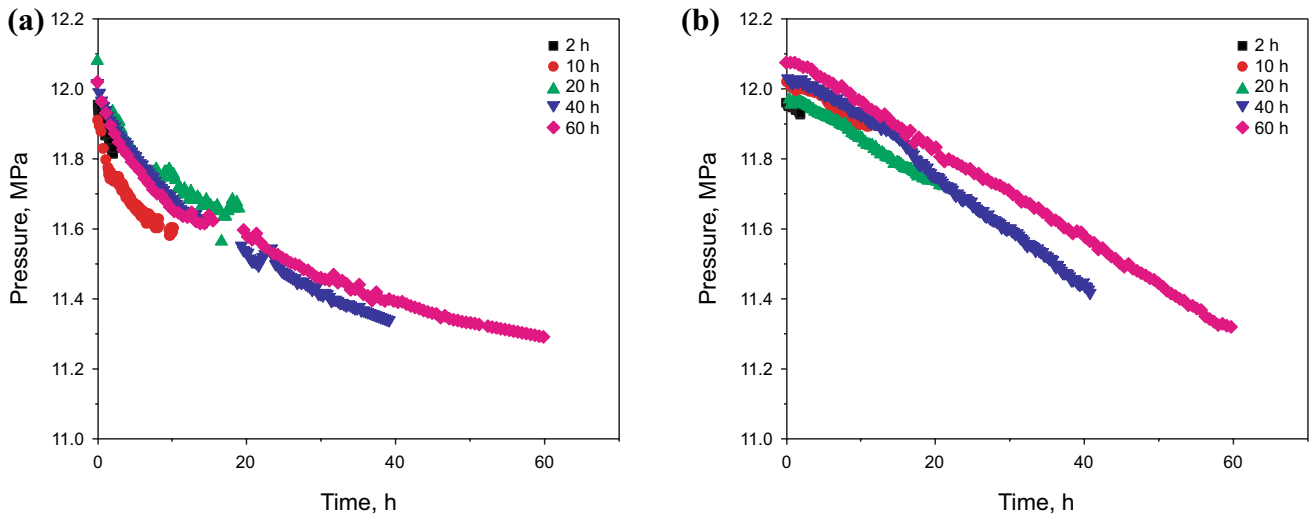

Fig. 17 Relationships between pressure and time at 12 MPa and 60 °C: **a** Shale 1; **b** Sandstone 1

References

Ahmad HM, Kamal MS, Mahmoud M, Shakil Hussain S, Abouelresh M, Al-Harthi MA. Organophilic clay-based drilling fluids for mitigation of unconventional shale reservoirs instability and formation damage. J Energy Res Technol. 2019;141(9):093102. https://doi.org/10.1115/1.4043248.

Burrows LC, Haeri F. A literature review of CO_2, natural gas, and water-based fluids for enhanced oil recovery in unconventional reservoirs. Energy Fuels. 2020;34(5):5331–80. https://doi.org/10.1021/acs.energyfuels.9b03658.

Busahmin BS, Maini BB. Effect of solution-gas-oil-ratio on performance of solution gas drive in foamy heavy oil systems. In: Canadian Unconventional Resources and International Petroleum Conference, 19–21 October 2010, Calgary, Alberta, Canada. doi:https://doi.org/10.2118/137866-MS.

Bustin AMM, Bustin RM. Importance of rock properties on the producibility of gas shales. Int J Coal Geol. 2012;103:132–47. https://doi.org/10.1016/j.coal.2012.04.012.

Chen C, Balhoff M, Mohanty KK. Effect of reservoir heterogeneity on primary recovery and CO_2 huff "n" puff recovery in shale-oil reservoirs. SPE Reserv Eval Eng. 2014;17(3):404–13. https://doi.org/10.2118/164553-PA.

Cherian BV, Stacey ES, Lewis R, Iwere FO, Heim RN, Higgins SM. Evaluating horizontal well completion effectiveness in a field development program. In: SPE Hydraulic Fracturing Technology Conference, 6–8 February 2012, Woodlands, TX. doi:https://doi.org/10.2118/152177-MS.

Cui X, Bustin AMM, Bustin RM. Measurements of gas permeability and diffusivity of tight reservoir rocks: different approaches and their applications. Geofluids. 2009;9(3):208–23. https://doi.org/10.1111/j.1468-8123.2009.00244.x.

Daneshy AA. Factors controlling the vertical growth of hydraulic fractures. In: SPE Hydraulic Fracturing Technology Conference, 19–21 January 2009, The Woodlands, Texas. doi:https://doi.org/10.2118/118789-MS.

Dong P, Liao X, Chen Z, Chu H. An improved method for predicting CO_2 minimum miscibility pressure based on artificial neural network. Adv Geo-Energy Res. 2019;3(4):355–64. https://doi.org/10.26804/ager.2019.04.02.

Du X, Gu M, Duan S, Xian X. The influences of CO_2 injection pressure on CO_2 dispersion and the mechanism of CO_2–CH_4 displacement in shale. J Energy Res Technol. 2018;140(1):012907. https://doi.org/10.1115/1.4037687.

Falk K, Pellenq R, Ulm FJ, Coasne B. Effect of chain length and pore accessibility on alkane adsorption in kerogen. Energy Fuels. 2015;29(12):7889–96. https://doi.org/10.1021/acs.energyfuels.5b02015.

Gamadi TD, Sheng JJ. Soliman MY, Menouar H, Watson MC, Emadibaladehi H. An experimental study of cyclic CO_2 injection to improve shale oil recovery. In: SPE Improved Oil Recovery Symposium, 12–16 April 2014, Tulsa ,Okahoma ,USA. doi:https://doi.org/10.2118/169142-MS.

Gaswirth SB, Marra KR. US Geological Survey 2013 assessment of undiscovered resources in the Bakken and Three Forks Formations of the US Williston Basin Province. AAPG Bull. 2015;99(4):639–60. https://doi.org/10.1306/08131414051.

Gaurav A, Dao E, Mohanty K. Evaluation of ultra-light-weight proppants for shale fracturing. J Pet Sci Eng. 2012;92:82–8. https://doi.org/10.1016/j.petrol.2012.06.010.

Gondiken S. Camurlu field immiscible CO_2 huff and puff pilot project. In: Middle East Oil Show, 7–10 March 1987, Bahrain. doi:https://doi.org/10.2118/15749-MS.

Hawthorne SB, Gorecki CD, Sorensen JA, Steadman EN, Harju JA, Melzer S. Hydrocarbon mobilization mechanisms from upper, middle, and lower Bakken reservoir rocks exposed to CO_2. In: SPE Unconventional Resources Conference Canada, 5–7 November 2013, Calgary, Alberta, Canada. doi:https://doi.org/10.2118/167200-MS.

Hawthorne SB, Miller DJ. Hydrocarbon recovery from williston basin shale and mudrock cores with supercritical CO2: part 1. Method validation and recoveries from cores collected across the basin. Energy Fuels. 2019;33(8):6857–66. https://doi.org/10.1021/acs.energyfuels.9b01177.

Henni A, Jaffer S, Mather AE. Solubility of N_2O and CO_2 in *n*-dodecane. Can J Chem Eng. 2010;74(4):554–7. https://doi.org/10.1002/cjce.5450740418.

Hoffman BT. Comparison of various gases for enhanced recovery from shale oil reservoirs. In: SPE Improved Oil Recovery Symposium, 14–18 April, 2012, Tulsa, Oklahoma, USA. doi:https://doi.org/10.2118/154329-MS.

Huang F, Xu R, Jiang P, Wang C, Wang H, Lun Z. Pore-scale investigation of CO_2/oil exsolution in CO_2 huff-n-puff for enhanced

oil recovery. Phys Fluids. 2020;32(9):092011. https://doi.org/10.1063/5.0021107.

Iddphonce R, Wang J, Zhao L. Review of CO_2 injection techniques for enhanced shale gas recovery: prospect and challenges. J Nat Gas Sci Eng. 2020;77:103240. https://doi.org/10.1016/j.jngse.2020.103240.

Iwere FO, Heim RN, Cherian BV. Numerical simulation of enhanced oil recovery in the middle bakken and upper three forks tight oil reservoirs of the Williston Basin. In: SPE Americas Unconventional Resources Conference, June 5–7 2012, Pittsburgh, PA. doi:https://doi.org/10.2118/154937-MS.

Jia B, Tsau J-S, Barati RJF. A review of the current progress of CO_2 injection EOR and carbon storage in shale oil reservoirs. Fuel. 2019;236:404–27. https://doi.org/10.1016/j.fuel.2018.08.103.

Kong B, Wang S, Chen S. Simulation and optimization of CO_2 huff-and-puff processes in tight oil reservoirs. In: SPE Improved Oil Recovery Conference, 11–13 April 2016, Tulsa, Oklahoma, USA. doi:https://doi.org/10.2118/191873-MS.

Kurniawan Y, Bhatia SK, Rudolph V. Simulation of binary mixture adsorption of methane and CO_2 at supercritical conditions in carbons. AIChE J. 2006;52(3):957–67. https://doi.org/10.1002/aic.10687.

Li L, Sheng JJ, Xu J. Gas selection for huff-n-puff EOR in shale oil reservoirs based upon experimental and numerical study. In: SPE Unconventional Resources Conference, 15–16 February 2017, Calgary, Alberta, Canada. doi:https://doi.org/10.2118/185066-MS.

Li L, Zhang Y, Sheng JJ. Effect of the injection pressure on enhancing oil recovery in shale cores during the CO_2 huff-n-puff process when it is above and below the minimum miscibility pressure. Energy Fuels. 2017;31(4):3856–67. https://doi.org/10.1021/acs.energyfuels.7b00031.

Li S, Li Z, Dong Q. Diffusion coefficients of supercritical CO_2 in oil-saturated cores under low permeability reservoir conditions. J CO2 Util. 2016;14:47–60. https://doi.org/10.1016/j.jcou.2016.02.002.

Li S, Li B, Zhang Q, Li Z, Yang D. Effect of CO_2 on heavy oil recovery and physical properties in huff-n-puff processes under reservoir conditions. J Energy Res Technol. 2018;140(7):072907. https://doi.org/10.1115/1.4039325.

Lu H. Petrochemical Basic Data Manual. Beijing: Chemical Industry Publishing House; 1982.

McGlade C, Speirs J, Sorrell S. Unconventional gas: a review of regional and global resource estimates. Energy. 2013;55:571–84. https://doi.org/10.1016/j.energy.2013.01.048.

Mitchell MC, Gallo M, Nenoff TM. Computer simulations of adsorption and diffusion for binary mixtures of methane and hydrogen in titanosilicates. J Chem Phys. 2004;121(4):1910–6. https://doi.org/10.1063/1.1766019.

Nguyen P, Carey JW, Viswanathan HS, Porter M. Effectiveness of supercritical-CO_2 and N_2 huff-and-puff methods of enhanced oil recovery in shale fracture networks using microfluidic experiments. Appl Energy. 2018;230:160–74. https://doi.org/10.1016/j.apenergy.2018.08.098.

Nieuwoudt I, Du Rand M. Measurement of phase equilibria of supercritical carbon dioxide and paraffins. J Supercrit Fluids. 2002;22(3):185–99. https://doi.org/10.1016/s0896-8446(01)00122-x.

Okiongbo KS, Aplin AC, Larter SR. Changes in type II kerogen density as a function of maturity: Evidence from the Kimmeridge Clay Formation. Energy Fuels. 2005;19(6):2495–9. https://doi.org/10.1021/ef050194+.

Ottiger S, Pini R, Storti G, Mazzotti M. Competitive adsorption equilibria of CO_2 and CH_4 on a dry coal. Adorption. 2008;14(4):539–56. https://doi.org/10.1007/s10450-008-9114-0.

Pollastro RM, Cook TM, Roberts LNR, Schenk CJ, Lewan MJ, Anna LO. Assessment of undiscovered oil resources in the Devonian–Mississippian Bakken Formation, Williston Basin Province, Montana and North Dakota. United States Geological Survey United States Department of the Interior. 2008. doi:https://doi.org/10.1021/256154.

Radlinski AP, Mastalerz M. Application of SAXS and SANS in evaluation of porosity, pore size distribution and surface area of coal. Int J Coal Geol. 2004;59(3–4):245–71. https://doi.org/10.1016/j.coal.2004.03.002.

Sang Q, Li Y, Yang Z, Zhu C, Yao J, Dong M. Experimental investigation of gas production processes in shale. Int J Coal Geol. 2016;159:30–47. https://doi.org/10.1016/j.coal.2016.03.017.

Schenewerk P, Thomas J, Bassiouni Z, Wolcott J. Evaluation of a South Louisiana CO_2 huff'n'puff field test. In: SPE/DOE Enhanced Oil Recovery Symposium, 22–24 April 1992, Tulsa, Oklahoma. doi:https://doi.org/10.2118/24143-MS.

Sharma S, Sheng JJ. A comparative study of huff-n-puff gas and solvent injection in a shale gas condensate core. J Nat Gas Sci Eng. 2017;38:549–65. https://doi.org/10.1016/j.jngse.2017.01.012.

Sheng JJ. Enhanced oil recovery in shale reservoirs by gas injection. J Nat Gas Sci Eng. 2015;22:219–29. https://doi.org/10.1016/j.jngse.2014.12.002.

Sheng JJ. Optimization of huff-n-puff gas injection in shale oil reservoirs. Petroleum. 2017;3(4):562–8. https://doi.org/10.1016/j.petlm.2017.03.004.

Singh H. Impact of four different CO_2 injection schemes on extent of reservoir pressure and saturation. Adv Geo-Energy Res. 2018;2(3):305–18. https://doi.org/10.26804/ager.2018.03.08.

Sing KSW, Everett DH, Haul RAW, Moscou L, Pierotti RA, Rouquerol J, et al. Reporting physisorption data for gas/solid systems. Weinheim: Wiley; 1985. https://doi.org/10.1085/658154.s.

Su X, Yue X-A, Moghanloo RG. Interplay between rock permeability and the performance of huff-n-puff CO_2 injection. ACS Omega. 2020;5(27):16575–83. https://doi.org/10.1021/acsomega.0c01343.

Tan Y, Pan Z, Liu J, Feng X-T, Connell LD. Laboratory study of proppant on shale fracture permeability and compressibility. Fuel. 2018;222:83–97. https://doi.org/10.1016/j.fuel.2018.02.141.

Tong J, Han X, Wang S, Jiang X. Evaluation of structural characteristics of Huadian oil shale kerogen using direct techniques (solid-state ^{13}C NMR, XPS, FT-IR, and XRD). Energy Fuels. 2011;25(9):4006–13. https://doi.org/10.1021/ef200738p.

Torabi F, Asghari K. Effect of operating pressure, matrix permeability and connate water saturation on performance of CO_2 huff-and-puff process in matrix–fracture experimental model. Fuel. 2010;89(10):2985–90. https://doi.org/10.1016/j.fuel.2010.05.020.

Tovar FD, Barrufet MA, Schechter DS. Gas injection for EOR in organic rich shale. Part I: operational philosophy. In: SPE Improved Oil Recovery Conference, 14–18 April 2018, Tulsa, Oklahoma, USA. doi:https://doi.org/10.2118/190323-MS.

Wan T, Sheng JJ, Soliman M. Evaluate EOR potential in fractured shale oil reservoirs by cyclic gas injection. In: SPE/AAPG/SEG Unconventional Resources Technology Conference, 12–14 August 2013, Denver, Colorado, USA. doi:https://doi.org/10.1190/urtec2013-187.

Wang B. Research on hydricarbon generation potential of Chang-7 member in Yanchan Formation. Ordos Basin Pet Geol Eng. 2015;29(4):27–30. https://doi.org/10.1111/j.1755-6724.2008.tb00623.x.

Wang J, Gu D, Guo W, Zhang H, Yang D. Determination of total organic carbon content in shale formations with regression analysis. J Energy Res Technol. 2019;141(1):012907. https://doi.org/10.1115/1.4040755.

Wang Z, Ma J, Gao R, Zeng F, Huang C, Tontiwachwuthikul P, et al. Optimizing cyclic CO_2 Injection for low-permeability oil

reservoirs through experimental study. In: SPE Unconventional Resources Conference Canada, 5–7 November 2013, Calgary, Alberta, Canada. doi:https://doi.org/10.2118/167193-MS.

Xie X, Li M, Littke R, Huang Z, Ma X, Jiang Q, et al. Petrographic and geochemical characterization of microfacies in a lacustrine shale oil system in the Dongying Sag, Jiyang Depression, Bohai Bay Basin, eastern China. Int J Coal Geol. 2016;165:49–63. https://doi.org/10.1016/j.coal.2016.07.004.

Yang ZH, Wang WH, Dong MZ, Wang JJ, Li YJ, Gong HJ, et al. A model of dynamic adsorption-diffusion for modeling gas transport and storage in shale. Fuel. 2016;173:115–28. https://doi.org/10.1016/j.fuel.2016.01.037.

Yu W, Lashgari H, Sepehrnoori K. Simulation study of CO_2 huff-n-puff process in Bakken tight oil reservoirs. In: SPE Western North American and Rocky Mountain Joint Regional Meeting, April 16–18 2014, Denver, Colorado, USA. doi:https://doi.org/10.2118/169575-MS.

Yu W, Lashgari HR, Wu K, Sepehrnoori K. CO_2 injection for enhanced oil recovery in Bakken tight oil reservoirs. Fuel. 2015;159(1):354–63. https://doi.org/10.1016/j.fuel.2015.06.092.

Yu Y, Sheng JJ. An experimental investigation of the effect of pressure depletion rate on oil recovery from shale cores by cyclic N_2 injection. In: Unconventional Resources Technology Conference, 20–22 July 2015, San Antonio, Texas, USA. doi:https://doi.org/10.15530/urtec-2015-2144010.

Yu Y, Sheng JJ. A comparative experimental study of IOR potential in fractured shale reservoirs by cyclic water and nitrogen gas injection. J Pet Sci Eng. 2016;149:844–50. https://doi.org/10.1016/j.petrol.2016.11.034.

Zhang Y, Yu W, Li Z, Kamy S. Simulation study of factors affecting CO_2 huff-n-puff process in tight oil reservoirs. J Pet Sci Eng. 2018;163:264–9. https://doi.org/10.1016/j.petrol.2017.12.075.

Zheng S, Yang D. Experimental and theoretical determination of diffusion coefficients of CO_2-heavy oil systems by coupling heat and mass transfer. J Energy Res Technol. 2017;139(2):022901. https://doi.org/10.1115/1.4033982.

Zhu C, Dong M, Gong H. Competitive adsorption behaviors of carbon dioxide and *n*-dodecane mixtures in 13X molecular sieve. IOP Conf Ser Earth Environ Sci. 2018. https://doi.org/10.1088/1755-1315/108/2/022079.

Zhu C, Li Y, Gong H, Sang Q, Li Z, Dong PM. Adsorption and dissolution behaviors of carbon dioxide and *n*-dodecane mixtures in shale. Energy Fuels. 2018;32(2):1374–86. https://doi.org/10.1021/acs.energyfuels.7b03417.

Zhu C, Li Y, Zhao Q, Gong H, Sang Q, Zou H, Dong M, et al. Experimental study and simulation of CO_2 transfer processes in shale oil reservoir. Int J Coal Geol. 2018;191:24–36. https://doi.org/10.1016/j.coal.2018.03.002.

Zhu C, Qin X, Li Y, Gong H, Li Z, Xu L, Dong MJF, et al. Adsorption and dissolution behaviors of CO_2 and n-alkane mixtures in shale: effects of the alkane type, shale properties and temperature. Fuel. 2019;253:1361–70. https://doi.org/10.1016/j.fuel.2019.05.002.

Zou Y, Yang Z. Formation mechanism, geological characteristics and development strategy of nonmarine shale oil in China. Pet Explor Dev. 2013;40(1):14–26. https://doi.org/10.1016/S1876-3804(13)60002-6.